Dispersion of Fine Primary Inclusions of MgO and ZrO_2 in Fe-10 Mass Pct Ni Alloy and the Solidification Structure

KIMIAKI SAKATA and HIDEAKI SUITO

The homogeneous dispersion of primary inclusions of MgO and ZrO_2 was studied in an Fe-10 mass pct Ni alloy as a function of the holding time at 1873 K and the cooling rate. The spatial size distribution was estimated from the planar size distribution obtained in a cross section by applying the Schwartz–Saltykov transformation. It was found that the content of insoluble Mg or Zr estimated from the size distribution agreed with that obtained from chemical analysis. The influence on the solidification macrostructure such as columnar dendrite, equiaxed dendrite, and globular crystal of dissolved Mg or Zr and inclusion particles having the mean diameter of roughly 1 μm was investigated. The area fraction of globular crystals in the Mg deoxidation decreased with increasing dissolved Mg content (>30 mass ppm) in the presence of MgO particles. In the Zr deoxidation, however, globular crystals were only observed in the presence of ZrO_2 particles without respect to the presence of dissolved Zr.

I. INTRODUCTION

THE high number of nonmetallic inclusions, which will not go into solution at elevated temperatures, may effectively hinder grain growth. Thus, the positive use of primary deoxidation products is considered to be one of the challenging techniques for improving the mechanical properties of steel, such as strength and toughness. In order to introduce fine primary inclusions into a liquid steel homogeneously, a complete understanding of the major controlling factors such as coalescence and separation of inclusions during cooling and subsequent solidification of steel is required. It was confirmed in our previous experiments[1] that the primary inclusions having the mean diameter of roughly 1 μm could be obtained by (1) using a strong deoxidant, (2) reducing the time when the particles were in a fluid or partly fluid state, and (3) choosing a proper solidification rate. These findings can be explained as follows. A strong deoxidant increases the degree of supersaturation for oxide precipitation, which leads to an increase of the inclusion number. The FeO-containing particles have higher wettability, thus leading to the particle coalescence, but a strong deoxidant reduces the FeO content in the initial deoxidation product to a considerable degree.[1] Inclusion particles are not pushed out by the advancing liquid-solid interface, when the growth rate is above the critical value, thus resulting in the uniform distribution.

In order to elucidate the influence of inclusion particles on grain size control and their correlation with the mechanical properties, knowledge of particle size distribution is of crucial importance rather than that of a mean value. However, the data on size distribution can be validated only by comparing the volume fraction of particles, which can be obtained from the contents of oxygen and/or an insoluble element as inclusions, with that estimated from the microscopic inclusion count.

KIMIAKI SAKATA, Graduate Student, Department of Metallurgy, and HIDEAKI SUITO, Professor, Institute for Advanced Materials Processing, are with Tohoku University, Sendai 980-8577, Japan.

Manuscript submitted February 17, 1999.

It has been known that primary inclusions and dissolved elements influence the solidification micro- and macrostructures. Primary inclusions act as nuclei and thus increase the amount of globular crystals, depending on their chemical composition and crystallographic parameters. A dissolved element influences solidification microstructure through the degree of constitutional supercooling, the solid-liquid interfacial tension, and other aspects. Furthermore, oxide particles and dissolved elements, which are redistributed during solidification, have a strong influence on the kinetics of the subsequent solid-state transformation and precipitation kinetics.

In this investigation, an Fe-10 mass pct Ni alloy containing the initial oxygen of 70 to 160 mass ppm was deoxidized with an Ni-15 mass pct Mg alloy or an Fe-50 mass pct Zr alloy at 1873 K. The degree of dispersion of primary inclusion particles was studied as a function of holding time at 1873 K and cooling rate, on the basis of the measurement of size distribution in a planar cross section. Furthermore, the influence of the MgO or ZrO_2 particles and the dissolved Mg or Zr on the solidification structure was investigated. The results for the grain growth observed at 1673 K are reported elsewhere.[2]

II. EXPERIMENTAL

A. *Procedure*

1. *Mg deoxidation*

Deoxidation experiments were carried out in an induction furnace (100 kHz) with a graphite susceptor. The temperature was controlled by a PID controller and was measured by a Pt-6 mass pct Rh / Pt-30 mass pct Rh thermocouple within $\pm$5 K. A charge was prepared by mixing high-purity electrolytic iron (99.99 mass pct) and globular nickel (99.97 mass pct) to obtain an overall composition of Fe-10 mass pct Ni. The initial oxygen content was controlled by keeping the holding time at 1873 K (1 hour), the gas flow rate, and the size of added electrolytic Fe constant. The sample (70 g) was melted at 1873 K in an Al_2O_3 or MgO crucible under

a deoxidized Ar atmosphere (200 mL/min). Then, the melt was held for 30 minutes and was sampled by using a quartz tube for the analysis of initial oxygen contents (70 to 160 mass ppm). An Ni-15 mass pct Mg alloy (0.75 g), which was prepared by premelting in an induction furnace, was added and immediately the melt was stirred manually by an Al_2O_3 rod for 30 seconds for homogenization in order not to attach the rod to the crucible wall. The sample was kept for a certain time (0 to 60 minutes) for the purpose of controlling the inclusion size and number, and then was cooled to 1673 K at the rate of 0.08, 0.18, and 0.70 K/s by using the PID program controller. The cooling rate was determined from the slope of a cooling curve. The sample was kept for 0 to 120 minutes at 1673 K, followed by quenching in water.

2. *Zr deoxidation*

An Fe-10 mass pct Ni alloy (70 g) was melted at 1873 K in an Al_2O_3 or ZrO_2 crucible under an Ar-7 vol pct H_2 (200 mL/min) atmosphere using an induction furnace (100 kHz). The initial oxygen content was controlled in the range between 80 and 130 mass ppm. Then, an Fe-50 mass pct Zr alloy (0.14 or 0.28 g), which was prepared by premelting in an arc furnace, was added and immediately the melt was stirred by an Al_2O_3 rod for 5 seconds. The melt was held for 0 to 60 minutes and then was cooled to 1673 K at the rate of 0.70 K/s. The sample was held for 0 to 120 minutes at 1673 K, followed by quenching in water.

B. *Estimation of Inclusion Size and Number*

The surface of a vertically sliced specimen was polished with 80 to 4000 grade emery paper, followed by final polishing with SiO_2 powder of 0.1 μm. Microphotographs were taken at 18 to 24 locations at each zone (top, middle, and bottom) of a polished cross section, and the particle sections and number of particles were observed at a magnification of 400 by using an optical microscope. The number of inclusion sections per unit area, N_A, was obtained from the measured number of particles for a given observed area. The observed area of each zone was 0.53 to 0.71 mm^2 except for experiments 1 and 11 (Table I). The diameter of particle sections, d_A, was estimated as the diameter of a circle with the same area of a sectioned inclusion. The particle section diameter of less than 0.5 μm could not be accurately measured at a magnification of 400. The reason for the use of this magnification was to observe the large area in a cross section. The errors for N_A and d_A arising from the oversight of small particle sections were estimated by assuming that the size distribution followed the log-normal function with the d_A = 1 μm and the standard deviation $\sigma = 0.5$. Consequently, if the particle sections of less than $d_A = 0.5$ μm were completely oversighted, the calculated $\bar{d}_A$ value was overestimated as 7.3 pct, and total N_A was underestimated as 10.9 pct against the true values. Similarly, if the particle sections of less than $d_A = 0.3$ μm were oversighted, $\bar{d}_A$ was overestimated as 0.8 pct and total N_A was underestimated as 1.03 pct. On the basis of these results, it can be said that the present values for $\bar{d}_A$ and N_A contain a few percent of overestimation and underestimation, respectively, against the true values. The inclusion composition was determined by a microprobe analysis.

The number and size of particle sections in a cluster were estimated as follows. The average number of particles in a cluster, $n_A^{(C)}$, was obtained as the arithmetic mean value of particle numbers in more than 50 clusters in a cross section. For the measurement of the number of clusters per unit area, N_A^C, 50 microphotographs were taken for each zone of top, middle, and bottom of the sliced specimen by using a magnification of 400. The size of each particle section in a cluster, $\bar{d}_A^{(C)}$, which was measured by a magnification of 1000, was calculated as the arithmetic mean value of more than 30 clusters.

C. *Cooling Curve*

The time/temperature curve was measured at the rate of 1.0 K/s, using a Pt-6 mass pct Rh/Pt-30 mass pct Rh thermocouple (0.3 mmϕ) in two alumina protection tubes (4 mmϕ) located at the center and rim parts of the sample (70 g). The arrest time, θ_f, which corresponds to the start and finish of solidification, was obtained from the change of the slope in a cooling curve.

D. *Solidification Structure*

In order to study the behavior of inclusion dispersion during solidification, the following method was used. The inclusion particles in a polished cross section could not be observed after etching in an Oberhoffer solution. Therefore, a mark was made by scratching a polished cross section prior to etching. The correlation between particle distribution and solidification microstructure was studied by superimposing the photomicrographs taken before and after etching at the marked region of a cross section.

The primary and secondary dendrite arm spacings of columnar dendrite and the spacing of globular crystals of more than 100 crystals were measured as a function of the distance from the crucible wall. The area fraction of globular crystals was measured by tracing the columnar dendrite, equiaxed dendrite, and globular crystal using a semiautomatic image analyzer.

E. *Chemical Analysis*

The contents of total and initial oxygen were determined by using the inert gas fusion-infrared absorptiometry within the accuracy of ± 3 pct (relative standard deviation (RSD)). The content of total nitrogen was determined by using the steam distillation-ion chromatography method within ± 2 pct (RSD). The contents of total Zr, Mg, and Al were obtained as follows. The contents of acid soluble Zr, Mg, and Al in metal were determined by inductively coupled plasma (ICP) emission spectrometry. Acid insoluble Zr, Mg, and Al was analyzed by the ICP method coupled with alkali fusion. The total content was obtained from the sum of the acid soluble and insoluble contents. The contents of insoluble Zr, Mg, and Al as inclusions were obtained as follows. The inclusions in 0.3 to 0.4 g of metal specimen were extracted under a controlled potential electrolysis using the nonaqueous electrolyte of 4 vol pct methylsalicylate - 1 wt pct salicylic acid - 1 wt pct TMAC-methanol. The residue on the membrane filter was fused with alkali fluxes and dissolved with dilute HCl. The contents of Zr, Mg, and Al, which correspond to insoluble Zr, Mg, and Al contents, were determined by the

Table I. Experimental Conditions, Inclusion Characteristics, and Metal Composition

Experiment Number	Holding Time 1873 K (Min)	Holding Time 1673 K (Min)	Inclusion Composition	$\bar{d}_A$ (μm)	N_A (mm^{-2})	f_V (Pct)	n	S (mm^2)	Total M (Mass Ppm)	Total O (Mass Ppm)	Total Al (Mass Ppm)	Total N (Mass Ppm)	Insoluble M (Mass Ppm)	Insoluble Al (Mass Ppm)	Initial O (Mass Ppm)	Crucible
Mg deoxidation																
8-1	0	0	MgO	0.87	329	0.0294	524	1.60	150	49	39	—	82	<1	164	Al_2O_3
8-2	0	60	MgO	0.88	360	0.0230	577	1.60	133	40	68	—	64	<1	103	Al_2O_3
8-3	0	120	MgO	0.87	347	0.0348	554	1.60	197	47	133	—	97	<1	160	Al_2O_3
6-1	10	0	MgO	1.20	265	0.0262	423	1.60	73	49	124	—	73	<1	153	Al_2O_3
6-2	10	60	MgO	1.37	258	0.0416	412	1.60	120	67	65	—	116	<1	112	Al_2O_3
6-3	10	120	MgO	1.13	255	0.0273	406	1.60	86	51	145	—	76	<1	105	Al_2O_3
7-1	30	0	MgO*	1.58	124	0.0169	266	2.13	48	53	169	—	47	12	73	Al_2O_3
7-2	30	60	MgO*	1.72	94	0.0144	202	2.13	43	25	950	—	40	10	74	Al_2O_3
7-3	30	120	MgO*	1.66	115	0.0194	245	2.13	40	50	110	—	54	11	129	Al_2O_3
9-1	60	0	MgO	1.45	112	0.0151	240	2.13	40	35	—	—	42	—	94	MgO
9-2	60	60	MgO	1.33	107	0.0144	226	2.13	37	32	—	—	40	—	91	MgO
9-3	60	120	MgO	1.55	89	0.0172	188	2.13	31	29	—	—	48	—	91	MgO
10-1**	0	0	MgO*	1.30	290	0.0567	464	1.60	100	113	32	—	95	8	190	Al_2O_3
10-2†	0	0	MgO	1.39	140	0.0352	298	2.13	70	78	55	—	105	14	225	Al_2O_3
11-1	0	0	MgO	0.84	383	0.0330	452	1.18	162	44	—	—	92	—	148	MgO
11-2	10	0	MgO	1.17	321	0.0445	379	1.18	140	68	—	—	124	—	100	MgO
11-3	30	0	MgO	1.62	183	0.0345	216	1.18	118	40	—	—	96	—	124	MgO
Zr deoxidation																
1-1	0	0	ZrO_2	1.17	492	0.0675	314	0.64	1730	123	168	35	646	<1	111	Al_2O_3
1-2	0	60	ZrO_2	1.10	649	0.0740	414	0.64	2200	135	124	8	401	<1	125	Al_2O_3
1-3	0	120	ZrO_2	1.20	638	0.0450	407	0.64	2150	82	96	34	590	<1	105	Al_2O_3
2-1	0	0	ZrO_2	1.12	342	0.0406	545	1.60	1270	74	—	61	971	—	76	ZrO_2
2-2	0	60	ZrO_2	1.10	270	0.0356	430	1.60	1400	65	—	46	572	—	112	ZrO_2
2-3	0	120	ZrO_2	1.17	261	0.0236	416	1.60	1250	43	—	49	811	—	108	ZrO_2
0-1	30	0	ZrO_2	1.25	134	0.0416	284	2.13	673	76	—	46	525	—	119	ZrO_2
3-1	60	0	ZrO_2	1.37	109	0.0317	232	2.13	175	58	—	40	192	—	131	ZrO_2
3-2	60	60	ZrO_2	1.60	129	0.0255	275	2.13	188	41	—	24	198	—	85	ZrO_2
3-3	60	120	ZrO_2	1.59	126	0.0269	269	2.13	156	49	—	48	84	—	85	ZrO_2
4-1‡	0	0	ZrO_2	1.05	144	0.0148	231	1.60	535	27	1180	24	272	4	—	Al_2O_3
4-2‡	0	60	ZrO_2	1.08	123	0.0160	196	1.60	469	29	1060	18	212	<1	—	Al_2O_3
4-3‡	0	120	ZrO_2	1.23	141	0.0213	226	1.60	487	39	1140	11	156	2	—	Al_2O_3
5-1‡	0	0	ZrO_2	1.12	81	0.0208	129	1.60	1060	38	1180	38	490	<1	—	Al_2O_3
5-2‡	0	60	ZrO_2	1.10	85	0.0154	136	1.60	1270	28	1180	14	274	2	—	Al_2O_3
5-3‡	0	120	ZrO_2	1.32	169	0.0311	270	1.60	1060	57	1010	21	340	<1	—	Al_2O_3

*MgO, MgO-Al_2O_3
**Cooling rate 0.18 K/s
†Cooling rate 0.08 K/s
‡Al deoxidation.

ICP method. The contents of dissolved Zr, Mg, Al were obtained by subtracting the contents of insoluble Zr, Mg, and Al from the total contents of Zr, Mg, and Al. In some of the experiments (3-1, 3-2, 7-3, 9-1 through 9-3, and 10-2), the content of insoluble M was found to be greater than that of total M due to the error in chemical analysis. More details are given elsewhere.[2]

III. RESULTS AND DISCUSSION

The experimental conditions, the size and number of inclusions, and the metal composition are summarized in Table I. The symbols n and S represent the number of particles and the observed area in a planar cross section, respectively. The term "initial O" denotes the oxygen content before the addition of the deoxidant and T, and "total M" represents total Zr and total Mg in the experimental numbers 0 to 5 and 6 to 11, respectively. Because the degree of the removal of deoxidation products is dependent on the kind of deoxidant and the amount of deoxidant, there is no correlation between initial oxygen and total oxygen.

A. *Particle Coalescence*

1. *Effect of holding time*

In order to study the effect of holding time at 1873 K on particle coalescence, the melt after deoxidation was held for 0, 30, and 60 minutes and then was cooled to 1673 K at the rate of 0.70 K/s. The arithmetic mean diameter of particle sections, $\bar{d}_A$, in a cross section and the number of inclusion sections per unit area, N_A, which includes clustered sections, are plotted against holding time at 1873 K in Figure 1. The error bars represent the range between the maximum and the minimum values. It is seen that the $\bar{d}_A$ values increase and the N_A values decrease with holding time at 1873 K due to the coalescence of particles and the separation by flotation. The values for $\bar{d}_A$ and N_A for the top, middle, and bottom zones of the specimen were found to be nearly equal. This

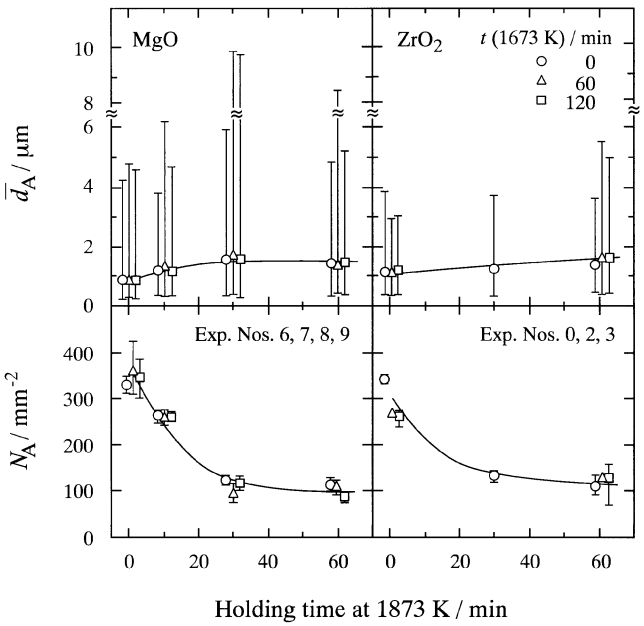

Fig. 1—Effect of holding time at 1873 K on size and number of inclusions.

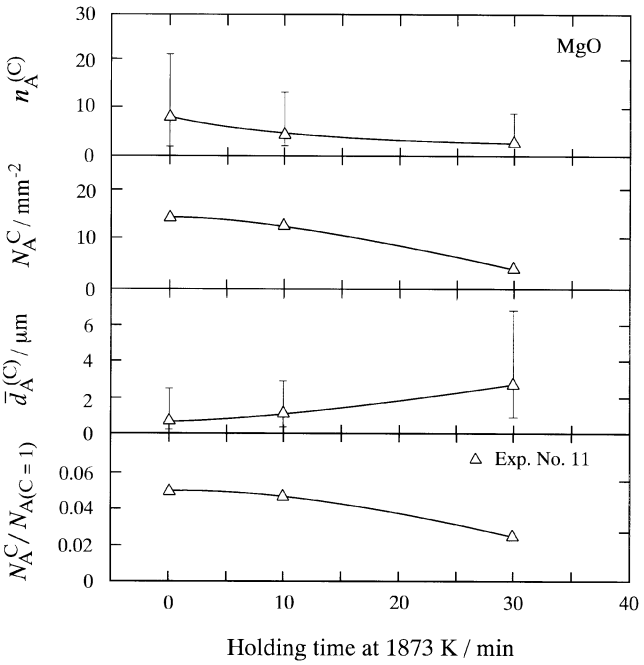

Fig. 2—Coalescence of particles as a function of holding time at 1873 K.

may be explained by the fact that after a few minutes holding time, large particles by coalescence float up rapidly and other particles tend to remain uniform due to the thermal convection. This suggests that particles are distributed uniformly. The N_A values decrease with holding time at 1873 K due to the coalescence and flotation, but they are not related to the initial oxygen level. The compositions of inclusion for the Mg and Zr deoxidation were observed to be MgO and MgO-Al_2O_3 and ZrO_2, respectively. More details concerning the inclusion composition will be given later in this section.

Many clustered inclusions, which were formed immediately after the addition of the deoxidant, were observed in the top surface region of the specimen. The degree of particle removal by flotation as a function of holding time at 1873 K can be seen from the values for the volume fraction of particles, f_V, obtained by chemical analysis, which are given in Table I. The calculation method for f_V values will be described in Section D–2. Because dissolved Mg reacted with an alumina crucible at holding time of 30 minutes at 1873 K (experiment 7), the f_V value in this case does not correspond to the degree of removal. The coarsening behavior by the mechanism of Ostwald ripening did not take place in the solid state, because the $\overline{d}_A$ and N_A values for a given holding time at 1873 K were not dependent on holding time at 1673 K, as shown in Figure 1.

The coalescence of particles as a function of holding time at 1873 K was discussed in view of cluster formations as follows. The number of particle sections in a cluster, $n_A^{(C)}$, the number of clusters per unit area, N_A^C, the particle section diameter in a cluster, $\overline{d}_A^{(C)}$, and the $N_A^C/N_{A(C=1)}$ ratio ($N_{A(C=1)}$ denotes the number of particle sections per unit area, assuming that a cluster is regarded as one particle section) were measured as a function of holding time at 1873 K in the Mg deoxidation experiments. These results are shown in Figure 2, in which the data were obtained in the experiments where the melt was cooled to 1673 K and immediately was quenched in water.

The number of particle sections in a cluster, $n_A^{(C)}$, decreases and the particle section diameter in a cluster, $\overline{d}_A^{(C)}$, increases with an increase in holding time. A cluster observed at zero holding time at 1873 K consists of about 20 particles at maximum, where the mean section diameter is less than 1 μm. The mean section diameter in a cluster at 30 minutes increases up to about 3 μm, and the number of particle sections in a cluster, $n_A^{(C)}$, and the number of cluster per unit area, N_A^C, decrease to a considerable extent. These observations suggest that particles in a cluster coagulate by a sintering mechanism and at the same time a cluster itself coarsens through the collision with particles and/or other clusters. The degree of clustering expressed by the $N_A^C/N_{A(C=1)}$ ratio at 0 minute is about 0.05, but it decreases to 0.03 after 30 minutes. In order to obtain more accurate information on cluster formation, the three-dimensional observation is preferable; that is, the clusters on a filter paper after electrolytic extraction should be observed by choosing a membrane filter with a proper pore size, which depends on cluster size. The cluster formation in the Zr deoxidation experiments was not analyzed in this study.

The inclusion composition in the Mg deoxidation experiments, where an Al_2O_3 crucible was used, was studied as a function of holding time at 1873 K using a microprobe analysis. The inclusions consisted of MgO in the range of holding time of less than 10 minutes, but at 30 minutes, about 40 pct of inclusions consisted of the mixture of MgO and Al_2O_3, where the Al_2O_3 content varied from a few to 100 pct. The reason for the formation of MgO-Al_2O_3 inclusions is not certain. However, the following mechanisms are considered: (1) Dissolved Mg reacts with crucible alumina to give Mg aluminates, (2) dissolved Al originating from the reaction of dissolved Mg with an Al_2O_3 crucible reacts with suspended MgO particles, and (3) Al_2O_3 particles resulting from Al reoxidation coalesce with MgO particles by collision.

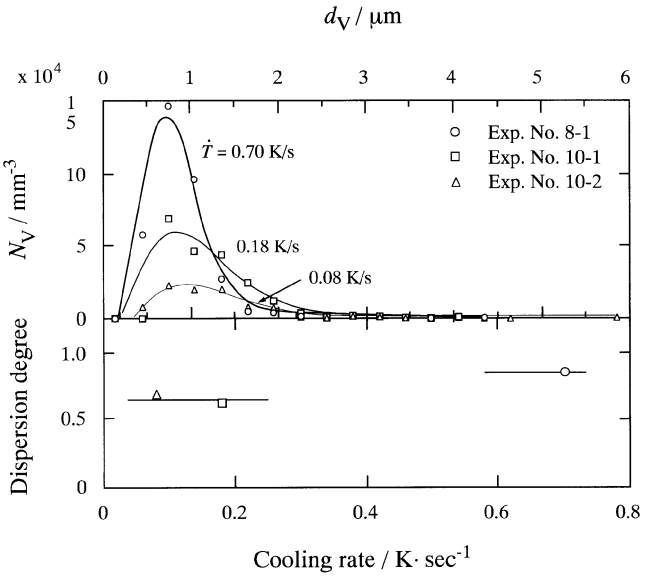

Fig. 3—Spatial size distribution and the degree of inclusion dispersion in dendritic solidification as a function of cooling rate in Mg deoxidation experiments.

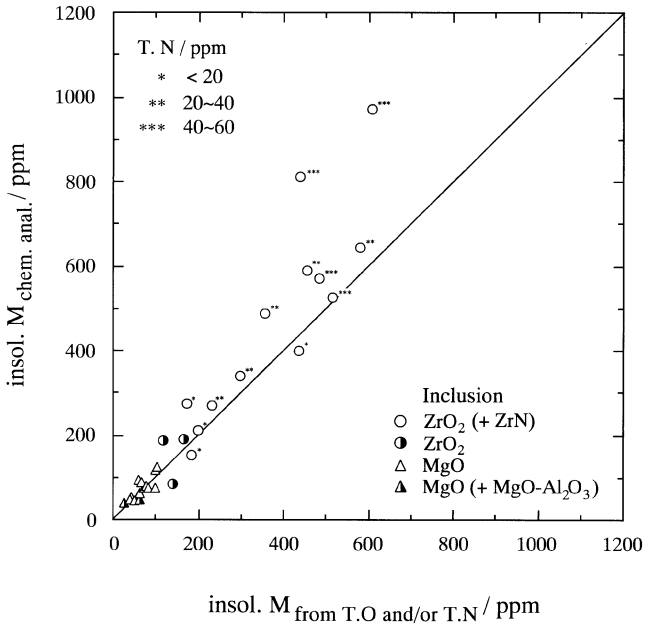

Fig. 4—Comparison of the analyzed content of insoluble M (Zr, Mg) from chemical analysis and that calculated from total O and total N contents.

2. *Effect of cooling rate*

The inclusion coalescence during cooling and the behavior of inclusion dispersion during subsequent solidification have been studied in the Mg deoxidation experiments (8-1, 10-1, and 10-2), where the melt was immediately cooled after Mg addition from 1873 to 1673 K at the rates of 0.08, 0.18, and 0.70 K/s. The spatial size distribution, which was obtained by applying the Schwartz–Saltykov transformation[3] to the planar size distribution, is shown in the upper diagram of Figure 3. More details on the results of this transformation will be explained in Section III–C. It was found that the number of inclusions decreased and the mean size increased with decreasing cooling rate. The inclusion composition obtained at $T = 0.70$ K/s was MgO, but some inclusions consisting of MgO-Al_2O_3 mixture were observed at $T = 0.08$ and 0.18 K/s. The time from 1873 K to the melting point (1773 K) of an Fe-10 mass pct Ni alloy was calculated as 30, 15, and 3 minutes for $T = 0.08$, 0.18, and 0.70 K/s, respectively. These results along with those shown in Figure 2 indicate that the coalescence and separation of particles occur more easily, when the sample is in a molten state. In addition to this, the coalescence becomes more favorable with a decrease in the solidification rate, because the particles, which are pushed out toward the interdendritic region, tend to coalesce, as observed in the following experiments.

The effect of the cooling rate on the particle distribution during solidification was studied in the Mg deoxidation experiments. The following technique was used for this purpose. The photomicrograph was first taken for the particles distributed for a given observed area, in which a mark was made by scratching. This was superimposed with another photomicrograph showing the revealed columnar dendrite by etching. By doing so, the degree of dispersion defined by the $(n/A)/(n_o/A_o)$ ratio was estimated, where the value of n_o is the number of particles for a given observed area, A_o, and n is the number of particles on the total area, A, of the etched columnar dendrite. In this study, the total observed area for A_o was 0.89 mm^2 and A/A_o was about 0.6. These results are shown in the lower diagram of Figure 3, indicating that the degree of dispersion tends to approach unity with increasing the cooling rate, but it is 0.6 in the rate of $T <$ 0.2 K/s. It can be said, therefore, that particles are dispersed almost uniformly at $T = 0.70$ K/s, but not in the range of $T < 0.2$ K/s, due to the pushing out effect by the advancing solid-liquid interface. The inclusions observed in the interdendritic spaces are found to be enriched and tend to be in a cluster. It can be concluded that the melt should be cooled immediately after addition of the deoxidant and the cooling rate above the critical value should be chosen in order to have uniform dispersion of particles.

B. *Insoluble Mg (Zr) and Total Oxygen*

The content of insoluble Mg or Zr obtained from chemical analysis is plotted against that calculated from the content of total oxygen and total nitrogen based on a simple stoichiometric calculation in Figure 4. The content of insoluble Zr was obtained from the sum of the content of insoluble Zr as ZrO_2 estimated from the total oxygen content and that of insoluble Zr as ZrN estimated from the total nitrogen content. The asterisks represent the samples containing ZrN precipitates. In the Zr deoxidation experiments having a high content of dissolved Zr represented by three asterisks, the cuboidal ZrN particles with the size of 5 to 10 μm were observed mostly at the grain boundaries. This is attributed to the nitrogen pick up from Fe-50 mass pct Zr alloy. On the other hand, no ZrN precipitate was observed in the experiments having a very low content of dissolved Zr represented by half-filled marks.

The content of soluble nitrogen was calculated as 0.3 to 1.6 mass ppm using the solubility product [pct Zr] · [pct N] = 4.9×10^{-6}[4] at 1673 K in the range of the soluble Zr content between 300 and 1800 mass ppm. This indicates

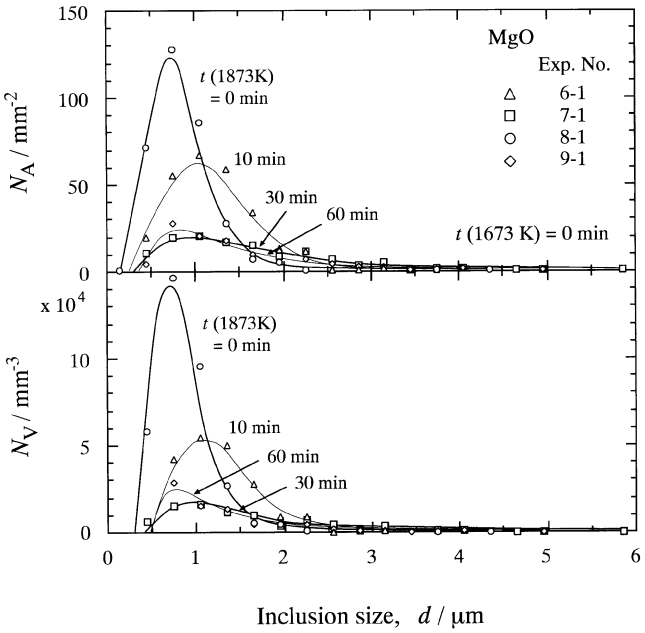

Fig. 5—Planar and spatial distribution curves as a function of holding time at 1873 K in Mg deoxidation.

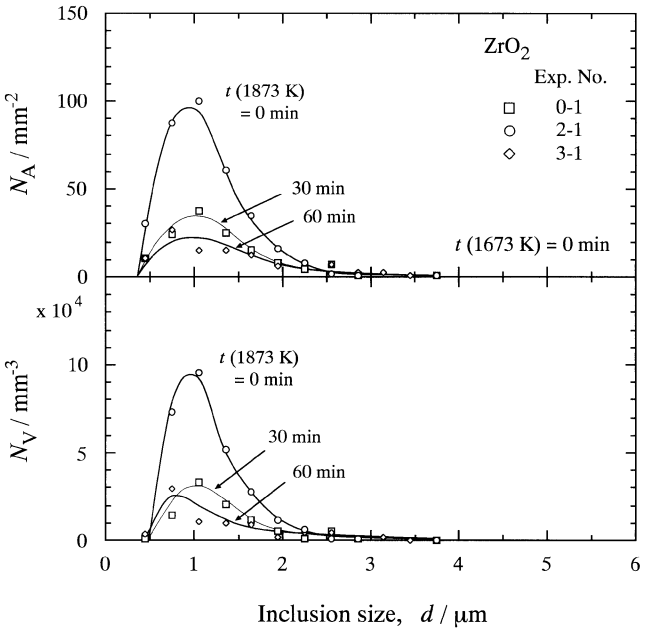

Fig. 6—Planar and spatial distributions curves as a function of holding time at 1873 K in Zr deoxidation.

that the previously mentioned assumption that total N content is equal to the insoluble N content as ZrN is reasonable. The calculation of insoluble Zr or Mg content from total oxygen content is justified, because the content of dissolved oxygen is negligibly small. In the case of the MgO-Al_2O_3 inclusion, the oxygen content as MgO was estimated by subtracting the oxygen content obtained by the insoluble Al content from total oxygen content. It can be seen from Figure 4 that the correspondence is fairly good except for two data points having a high content of total N. It follows that the method for the chemical analysis of insoluble Mg or Zr is accurate and thus the volume fraction of particles estimated from these values is considered to be valid.

C. *Particle Size Distribution*

The size distribution of inclusions was studied as a function of holding time at 1873 K in the Mg and Zr deoxidation experiments where the melt was cooled to 1673 K, followed by quenching in water. The planar size distributions of particles in a cross section of the Mg (experiments 6-1, 7-1, 8-1, and 9-1) and Zr (experiments 0-1, 2-1, and 3-1) deoxidation experiments are shown in the upper diagrams of Figures 5 and 6, respectively. The spatial size distributions obtained by the Schwartz–Saltykov method[3] with the step width of $\Delta = 0.3\ \mu$m are shown in the lower diagrams of Figures 5 and 6 for the Mg and Zr deoxidation experiments, respectively. It can be seen that the spatial size distribution curves are not significantly different from the planar size distribution curves except for the small size range.

In the Mg deoxidation, the N_A or N_V value at the mode diminishes regularly and the distribution curve becomes broad, showing an asymmetrical right-skewed curve, with an increasing holding time up to 30 minutes. These findings indicate that the particle coalescence occurs along with the particle separation with holding time, but relatively large particles tend to remain in the melt. In the Zr deoxidation, however, the N_A or N_V value at the mode continues to lower and the spread of the distribution curve at a large inclusion size is not wider compared with that observed in the Mg deoxidation. These results suggest that large particles are removed more rapidly compared with those in Mg deoxidation. This different behavior cannot be explained from the difference in the respective values for the density of $\rho_{ZrO_2} = 5.56$, $\rho_{MgO} = 3.65$, and $\rho_{Fe} = 7.89$ g/cm^3. It was found in the Zr deoxidation that precipitation of ZrO_2 occurs along the crucible wall with increasing holding time. This may be the probable reason for the decrease of the inclusion particles in the small size range. If the MgO particles in a cluster are more loosely packed, these agglomerates with a large size are apt to remain in the melt. Further study is required to clarify this different behavior.

In order to clarify the mechanism of the inclusion removal, the relationships between cumulative frequency and particle size are plotted in a probability graph for the planar size distribution, as shown in the upper diagrams of Figures 5 and 6. As a result, the log-normal distribution function was regarded as a better approximation for expressing the present data as a probability graph in comparison with the normal, exponential, and Rayleigh, which was used by Louat,[5] distribution functions. The results are plotted in the log-normal probability graph in Figure 7, in which an approximately linear relationship is obtained except for the data in the Zr deoxidation at 60 minutes. It can be seen from these results that the difference in the inclusion removal in the Mg and Zr deoxidation is more clearly demonstrated in the plot of the log-normal probability graph, as compared with the size distributions shown in Figures 5 and 6. That is, in the case of Mg deoxidation shown in the upper diagram of Figure 7, the shift of the line and the decrease of the slope with holding time suggest that the mean particle size and the width of the distribution curve increase with holding time. In the case of Zr deoxidation shown in the lower diagram, however, a small decrease of the slope implies that the

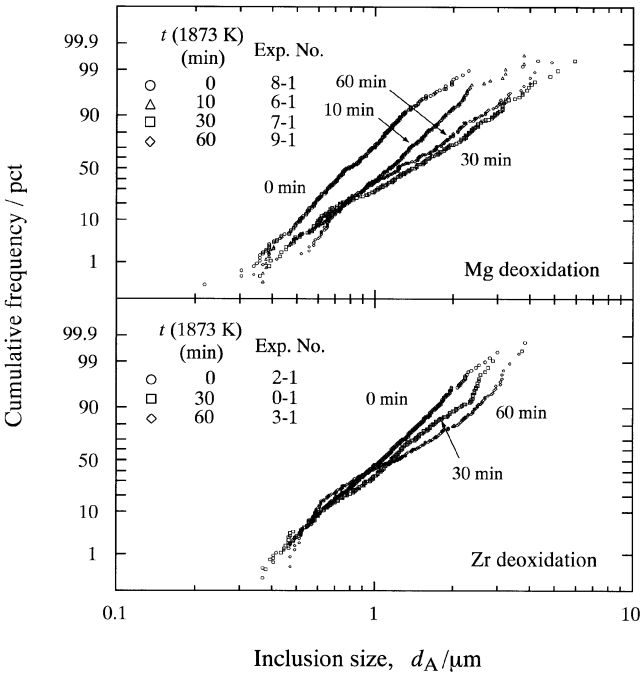

Fig. 7—Size distribution of inclusion particles in Mg and Zr deoxidation experiments in the log-normal probability graph.

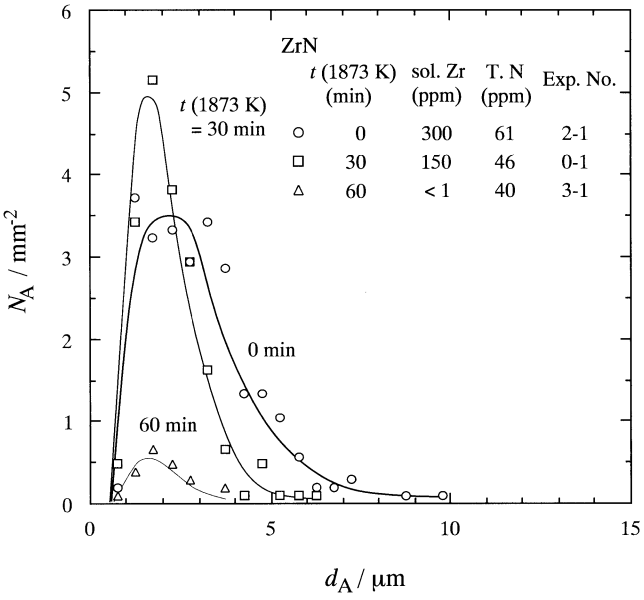

Fig. 8—Planar size distribution of ZrN particles in Zr deoxidation.

mean particle size remains unchanged, but the width of the distribution curve increases slightly with an increase of holding time.

The size distribution of ZrN in a planar cross section is shown in Figure 8 as a function of holding time at 1873 K. Total observed area was 10.5 mm^2 and the number of observed particles was 22 to 248. The content of dissolved Zr was observed to decrease with holding time due to the reaction with reducible oxide contained in a ZrO_2 crucible and/or to the reoxidation. In the case that the content of dissolved Zr was high (experiments 0-1 and 2-1), the ZrN particles with the maximum size of 5 to 10 μm precipitated at the grain boundaries and furthermore one ZrO_2 particle was located in the center of a ZrN precipitate; that is, the ZrO_2 particles act as a nucleant for the precipitation of ZrN. As will be explained in Section F, when the content of dissolved Zr and number of ZrO_2 particles are both high, one globular crystal revealed by etching is present within one austenite crystal grain. From this metallographic result, it could not be concluded whether ZrN precipitated in the interglobular crystal regions due to the enrichment of dissolved Zr and N during solidification or they precipitated along austenite grain boundaries during subsequent cooling after solidification. It is to be noted that the number of ZrN precipitates is extremely small compared with that of the ZrO_2 particle, as shown in Figure 6.

D. *Insoluble Mg (Zr) Content from Particle Size Distribution*

1. *Method for calculation of f_V*

The arithmetic mean of three-dimensional particle diameter, $\bar{d}_V$, can be expressed by Eq. [1], using the harmonic mean of two-dimensional particle diameter, $\bar{d}_{A(H)}$ $(=\{n/\sum_{i=1}^{n}(1/d_{A(i)})\})$[6], where $d_{A(i)}$ is the particle diameter in a cross section.

$$\bar{d}_V = (\pi/2) \cdot \bar{d}_{A(H)} \quad [1]$$

The number of particles per unit volume, N_V, can be given by the following relation:[6]

$$N_A = N_V \cdot \bar{d}_V \quad [2]$$

By substituting Eq. [1] into Eq. [2], we obtain

$$N_V = (2/\pi) \cdot (N_A/\bar{d}_{A(H)}) \quad [3]$$

where N_A is the number of particle sections per unit area.

The volume fraction of particle, f_V, is expressed as

$$f_V = (4/3)\ \pi \cdot (\bar{d}_V/2)^3 \cdot N_V \quad [4]$$

From Eqs. [1], [3], and [4], we have

$$f_V = (\pi^3/24) \cdot \bar{d}^2_{A(H)} \cdot N_A \quad [5]$$

In this article, the method in which f_V is estimated from Eq. [4] or [5] denotes the mean diameter method. It should be pointed out that the f_V value estimated from Eq. [4] or [5] is valid only in the case of monodispersed particles.[6] In the spatial size distribution shown in the lower diagrams of Figures 5 and 6, the volume fraction of the particle in each *i*th class, $f_{V(i)}$, with the step width of $\Delta = 0.3$ μm can be written as

$$f_{V(i)} = (4/3)\ \pi \cdot (d_{V(i)}/2)^3 \cdot N_{V(i)} \quad [6]$$

where $d_{V(i)}$ and $N_{V(i)}$ are the particle diameter and the number of particles per unit volume in the *i*th class in the spatial size distribution, respectively.

Then, f_V is given by

$$f_V = \sum_{i=1}^{k} f_{V(i)} \quad [7]$$

where k is the maximum number of size class.

In this article, the method of calculation of f_V from Eqs. [6] and [7] denotes the Schwartz–Saltykov method.

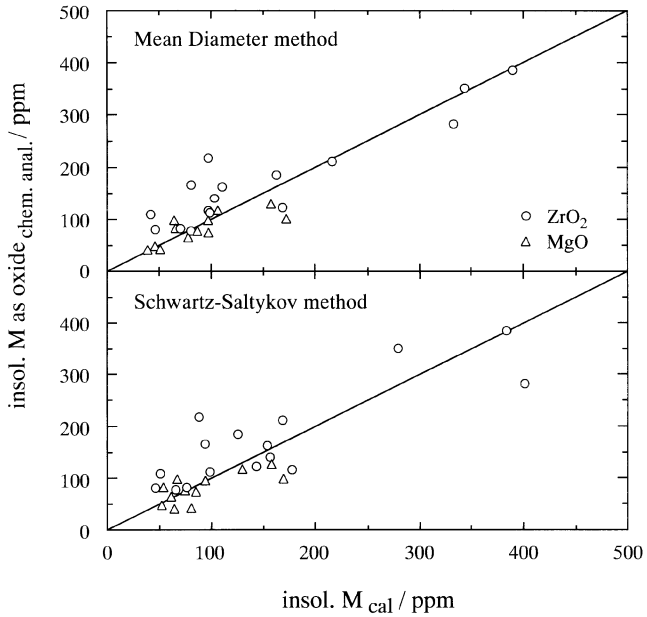

Fig. 9—Comparison of the content of insoluble M (Zr, Mg) as oxide from chemical analysis and that from Eq. [5] (upper diagram) and Eq. [7] (lower diagram).

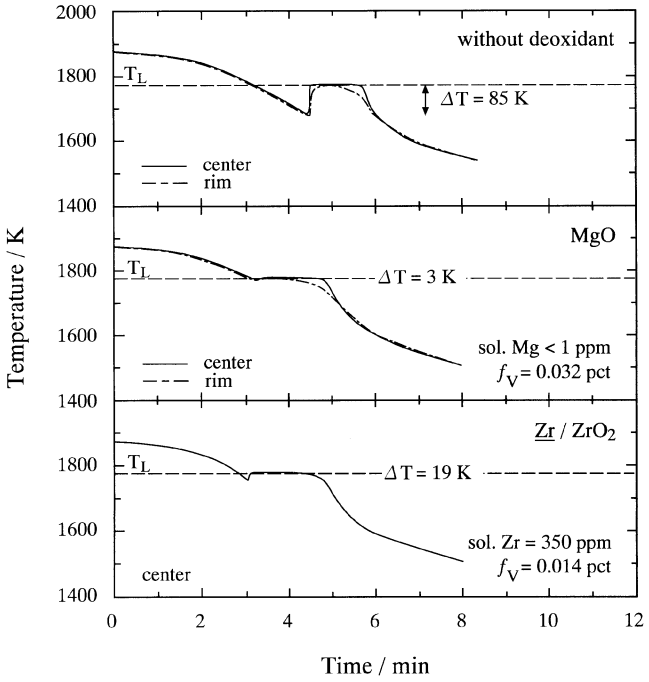

Fig. 10—Effects of particles and dissolved elements on the cooling curve.

2. *Comparison with insoluble M from chemical analysis*

The content of insoluble M (M = Mg, Zr) in mass ppm can be given by

$$[\text{ppm insoluble M}] = \frac{(f_V \cdot \rho_{MO_x}) \cdot (M_M/M_{MO_x}) \cdot 10^6}{f_V \cdot \rho_{MO_x} + (1 - f_V) \cdot \rho_{Fe}} \quad [8]$$

where M_M and M_{MO_x} represent the atomic weight of M and the molecular weight of MO_x, respectively, and ρ_i is the density of i species.

The values of f_V given in Table I for the Mg deoxidation were calculated from the analyzed contents of insoluble Mg by using Eq. [8]. However, the f_V values for the Zr deoxidation were calculated from the contents of insoluble Zr as ZrO_2 particles, which were obtained by subtracting the contents of insoluble Zr as ZrN from the analyzed contents of insoluble Zr. The values for $\bar{d}_A$ and N_A obtained in the Zr deoxidation in Table I correspond to those for oxide particles only.

The contents of insoluble Mg or Zr as oxide obtained from chemical analysis are plotted against those estimated from using Eqs. [5] and [8] in the upper diagram of Figure 9 for the data (experiments 0 to 9 except for experiment 7) given in Table I. The data points obtained in the Mg deoxidation are not included in Figure 9, because the inclusion composition is not MgO (experiments 7-1 to 7-3, 10-1, and 10-2). It is seen that a good correlation is observed except for a few data points in the Zr deoxidation. The contents of insoluble Mg or Zr as oxide obtained from chemical analysis are plotted against those estimated by using Eqs. [7] and [8] in the lower diagram of Figure 9, showing reasonable agreement with each other.

When particles have a size distribution, the f_V value estimated from the mean diameter method using Eq. [5] always leads to a smaller value compared with the true value, namely, the value obtained from chemical analysis.[7] This trend becomes obvious in the case that accurate measurements are carried out for the particles in the submicron range (*i.e.*, of $d_V < 1$ μm). In the present study, the particles below 0.5 μm could not be accurately measured, because a low magnification such as 400 was used in order to increase the observed area. This results in the overestimation of the $\bar{d}_{A(H)}$ value, as compared with the value for the true size distribution. Accordingly, a good correlation observed in the upper diagram of Figure 9 may be interpreted by the aforementioned offset effect.

In the case that the f_V value is estimated by using Eqs. [6] and [7], the f_V value tends to have a larger value, as compared with that for the true value, unless the size distribution in a large size range can be accurately measured. This is due to the fact that the f_V value is markedly increased by the presence of large particles even when their number is very small, that is, it increases with the cubed power of d_V, as is clear from Eq. [6]. However, because the size distribution was measured in a relatively large observed area using a low magnification, the size distribution in a large size range could be measured to a reasonable accuracy. This seems to be the reason that a good correlation was observed, as shown in the lower diagram of Figure 9. It is to be noted that the underestimation in the submicron range due to a low magnification has little effect on the f_V value.

E. *Effects of Particles and Dissolved Elements on the Cooling Curve*

The effects of inclusion particles and dissolved elements in the Mg and Zr deoxidation experiments on the degree of undercooling as well as the arrest time were studied in the measurement of a cooling curve at the rate of $T = 1.0$ K/s. The upper diagram of Figure 10 is the result for the experiments without deoxidation. Small suspended Al_2O_3

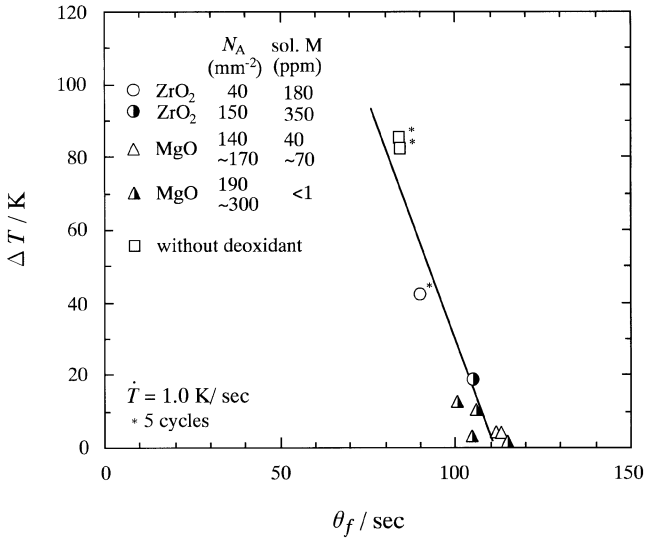

Fig. 11—Relation between degree of undercooling and arrest time in solidification.

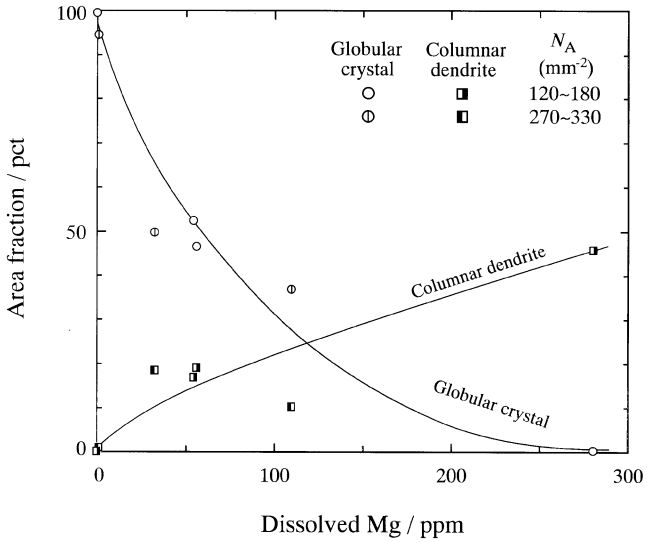

Fig. 12—Effect of dissolved Mg on solidification macrostructure in the presence of MgO particles.

particles originating from the Al_2O_3 crucible were coalesced by recycling the melting/solidification process five times to remove coagulated particles by flotation. The solid and dash-dotted lines correspond to the results measured by the thermocouples located in the center and the rim parts of the melt, respectively. As a result, the degree of undercooling, ΔT, was observed to be 85 K in both parts and the arrest time, θ_f, obtained at the rim is slightly shorter than that in the center.

The result for the Mg deoxidation using an Al_2O_3 crucible is shown in the middle diagram. The melt was held at 1873 K for more than 10 minutes to remove dissolved Mg by vaporization. It can be seen that the degree of undercooling is reduced and the arrest time increases, compared with the results without deoxidation. The excess growth of columnar dendrite originating from the crucible wall was observed in the experiments without deoxidation, while only equiaxed dendrite and globular crystal were observed in an entire cross-sectional area in the experiments with MgO particles (f_V = 0.032 pct) and very low content of dissolved Mg. The increase of the θ_f value in the presence of particles is interpreted by the fact that the solidification of globular crystals tends to occur adiabatically, thus resulting in a slow release of latent heat of fusion.

The lower diagram of Figure 10 shows one of the representative results for the Zr deoxidation experiments. The melt was first deoxidized with Al in an Al_2O_3 crucible, followed by separating inclusions for 30 minutes. It was confirmed from chemical analysis of insoluble Al that the Al_2O_3 particles were present to a negligibly small degree. Then, the melt was deoxidized with an Fe-50 mass pct Zr alloy. The ΔT value was found to be 19 K in the presence of dissolved Zr content (350 mass ppm) and ZrO_2 inclusions (f_V = 0.014 pct). In this case, only globular crystals were observed in an entire cross-sectional area.

The relationships between ΔT and θ_f are shown in Figure 11. It seems that the degree of undercooling decreases with an increase in the arrest time in solidification and the effect of inclusions on the decrease of the ΔT value is greater than that of dissolved M (M = Mg, Zr). More detailed systematic experiments are necessary in the future regarding the influence of particles and dissolved elements on this relationship.

F. *Solidification Structure*

In the present study, the columnar dendrite, equiaxed dendrite, and globular crystal were observed in the Mg deoxidation. The area fraction of globular crystal increased with decreasing the dissolved Mg content. In the Zr deoxidation, the globular crystal was only observed without respect to the dissolved Zr content. On the basis of these observations, the growth of the globular crystal can be explained by the inoculation effect of the deoxidation products.

1. *Without deoxidation*

Only columnar dendrites with the primary arm spacing of d_1 = 80 to 270 μm and arm length of l_1 = 3.5 to 13.2 mm, which originated from the crucible wall, were observed in the experiment without deoxidation. This is attributed to the narrow freezing range of 10 K in this alloy. The secondary dendrite arm spacing, d_2, was observed as 50 to 80 μm at 7 mm apart from the crucible wall. These results are in agreement with the previous observations for an Fe-30 mass pct Ni alloy.[8]

2. *Mg deoxidation*

The solidification macrostructure was studied in the Mg deoxidation experiments, in which the dissolved Mg content was controlled by changing the holding time at 1873 K and initial oxygen level. The melt was cooled to 1673 K at the rate of 0.70 K/s and immediately was quenched in water. The area fractions of globular crystal and columnar dendrite at the two inclusion numbers of N_A = 120 to 180 and 270 to 330 mm^{-2} are plotted against the content of dissolved Mg in Figure 12. The mean inclusion size was 1.0 to 1.5 μm. It can be seen that with increasing the content of dissolved Mg, the area fraction of globular crystals decreases, whereas that of columnar dendrite increases. The reason for a markedly well-developed columnar dendrite originating from the top surface may be interpreted by the steep temperature gradient caused by the exothermic reaction of Mg vaporization. Only globular crystals were observed in the presence

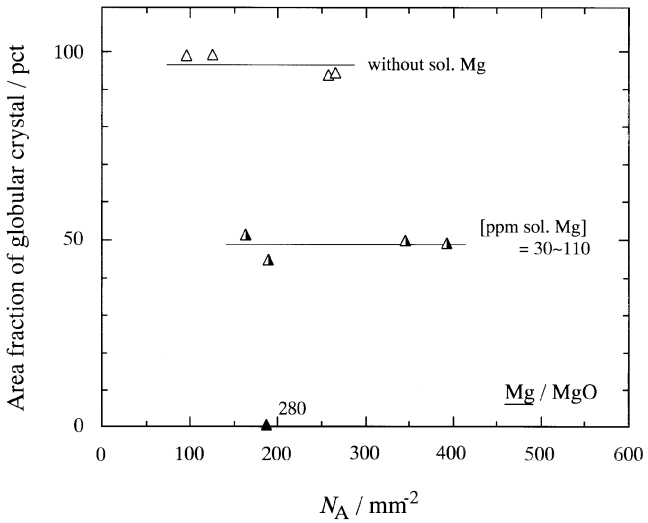

Fig. 13—Effect of number of inclusions on area fraction of globular crystal in Mg deoxidation.

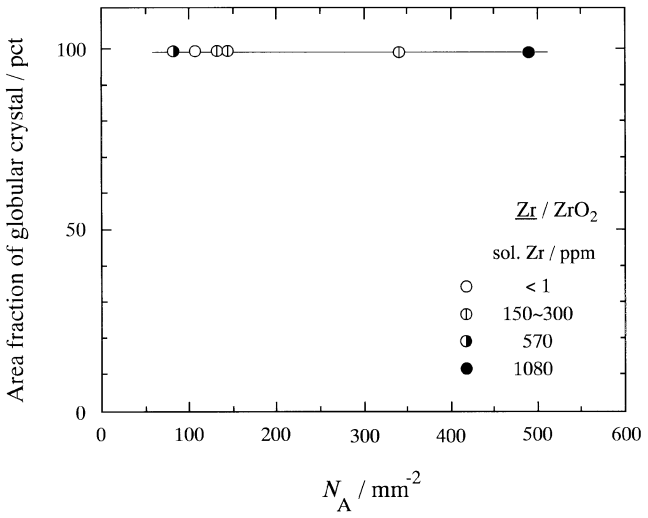

Fig. 14—Effect of number of inclusions on area fraction of globular crystal in Zr deoxidation.

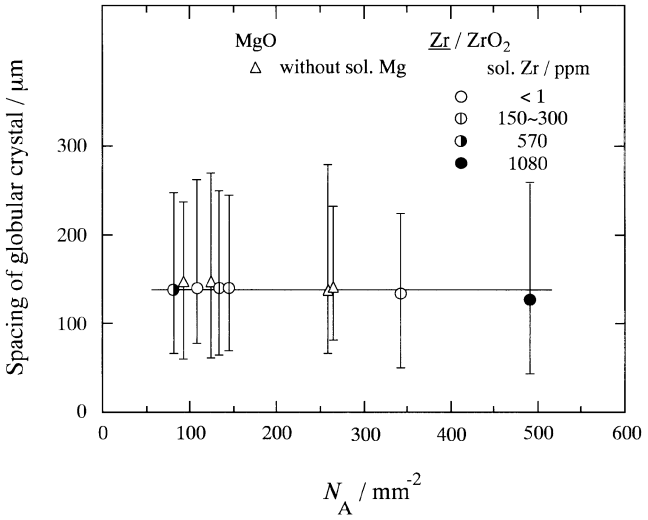

Fig. 15—Effect of number of inclusions on spacing of globular crystal.

of MgO inclusions, which act as nuclei, when the dissolved Mg content is negligibly small.

The effect of inclusion number on the area fraction of globular crystal was studied in the Mg deoxidation experiments and the results are shown in Figure 13 for a given dissolved Mg content. When the dissolved Mg content is high such as 280 mass ppm, no globular crystal was observed even in the presence of inclusions ($N_A = 180$ mm^{-2}). In the absence of dissolved Mg (< 1 mass ppm), only globular crystal was observed in the range of $N_A > 100$ mm^{-2}. In the presence of dissolved Mg containing 30 to 110 mass ppm, the area fraction of globular crystal was approximately 50 pct and the rest was the equiaxed and columnar dendrite in the range of $N_A > 150$ mm^{-2}. It is concluded on the basis of these results that for the complete formation of the globular crystal, the lowering of dissolved Mg is more effective in comparison with the increase in the number of MgO inclusions. Approximately 1 to 60 globular crystals etched by an Oberhoffer solution were revealed within one austenite crystal grain with the minimum diameter of 110 μm and the maximum diameter of 2 mm (the mean diameter of 800 μm). This was observed in an entire cross-sectional area.

3. *Zr deoxidation*

The effect of the number of ZrO_2 inclusions on the area fraction of globular crystal was studied as a function of dissolved Zr content. The results are shown in Figure 14. The data were obtained in experiments 0-1, 1-1, 2-1, 3-1, 4-1, and 5-1, where the melt was cooled to 1673 K at the rate of 0.70 K/s and immediately was quenched in water. It is apparent that only globular crystal is observed in the range of $N_A > 80$ mm^{-2}, regardless of the dissolved Zr level. This is completely a different behavior from that observed in the Mg deoxidation. From the practical viewpoint of obtaining the globular crystal, it is of interest to know the minimum level of N_A necessary for the globular crystal in the absence of dissolved Zr and the maximum level of dissolved Zr necessary for the globular crystal in the absence of ZrO_2 particles. One etched globular crystal was observed within one austenite crystal grain in the range of [mass ppm Zr] > 260 and $N_A > 80$ mm^{-2}. However, one austenite crystal grain with the minimum diameter of 100 μm and the maximum diameter of 900 μm (the mean diameter of 400 μm) consisted of about 1 to 30 of the globular crystal in the range of [mass ppm Zr] < 1 and $N_A = 110$ mm^{-2}.

The spacing of globular crystals in the Mg ([mass ppm Mg] < 1) or Zr deoxidation experiments, which were observed in an entire cross-sectional area, is plotted against the number of particles in Figure 15. The spacing of globular crystals was found to be independent of the content of dissolved Zr as well as the number of MgO and ZrO_2 particles. The approximately constant spacing of 130 μm was obtained in an entire cross-sectional area.

If one ZrO_2 particle acts as one nucleus for the globular crystal, the N_A value can be calculated as 15 mm^{-2} by substituting the mean spacing of a globular crystal of 130 μm into Δ_2 in the relation $\Delta_2 = 0.500 \cdot N_A^{-1/2}$,[9] where Δ_2 is the interparticle spacing in two dimensions. This N_A value is much smaller than that obtained for particles in the present deoxidation experiments ($N_A > 80$ mm^{-2}). This implies that

more than one particle is present within one globular crystal on the assumption that particles are homogeneously dispersed. If one particle of a deoxidation product effectively acts as one nucleus for the globular crystal and subsequent grain growth is strongly inhibited by a dissolved element, the spacing of the globular crystal will be expected to be the value of Δ_2 for a given N_A. In the present study, however, the spacing of globular crystal was independent of the number of particles and was independent of a dissolved element in the case of Zr deoxidation, as shown in Figure 15.

IV. CONCLUSIONS

Homogeneous dispersion of primary inclusions of MgO or ZrO_2 in an Fe-10 mass pct Ni alloy was studied at 1873 K, and the solidification structure was metallographically examined as a function of the number of inclusion particles and the dissolved Mg or Zr contents. The following conclusions were derived.

1. Due to the coalescence and flotation of particles, the $\overline{d}_A$ values increased and the N_A values decreased with increasing holding time at 1873 K or with decreasing cooling rate.
2. The spatial size distribution curves obtained by the Schwarz–Saltykov transformation were not significantly different from the planar size distribution curves. The distribution curves became broad with increasing holding time at 1873 K and the spread of the size distribution curve in the Mg deoxidation was found to be larger than that in the Zr deoxidation.
3. The content of insoluble Mg or Zr estimated from the planar size distributions agreed with that obtained by chemical analysis as a result of the accurate measurements of particle number in the large size range.
4. In the presence of dissolved Mg with more than 30 mass ppm, the excess development of the columnar dendrite from the top surface was observed. On the contrary, in the absence of dissolved Mg, equiaxed dendrite and globular crystals were observed in the presence of MgO particles.
5. Only globular crystals were observed in the presence of ZrO_2 particles without respect to the presence of dissolved Zr.

REFERENCES

1. A.V. Karasev and H. Suito: *Metall. Mater. Trans. B*, 1999, vol. 30B, pp. 259-70.
2. K. Sakata and H. Suito: Institute for Advanced Materials Processing, Tohoku University, Sendai, Japan, unpublished research, 1999.
3. E.E. Underwood: in *Quantitative Microscopy*, R.T. DeHoff and F.N. Rhines, eds., McGraw-Hill, Inc., New York, NY, 1968, pp. 149-200.
4. H. Chino and K. Wada: *Seitetsu-Kenkyu*, 1965, No. 251, pp. 5817-42.
5. N.P. Louat: *Acta Metall.*, 1974, vol. 22, pp. 721-24.
6. R.L. Fullman: *Trans. AIME*, 1953, vol. 197, pp. 447-52.
7. J. Takahashi and H. Suito: *CAMP-ISIJ*, 1997, vol. 10, p. 956.
8. Y. Kawashita and H. Suito: *Iron Steel Inst. Jpn.*, 1995, vol. 35, pp. 1459-67.
9. J. Gurland: in *Quantitative Microscopy*, R.T. DeHoff and F.N. Rhines, eds., McGraw-Hill, Inc., New York, NY, 1968, pp. 278-90.